

Flower-shaped NiMnO₃@NiCo₂S₄ heterojunction nanosheets for high-performance asymmetric supercapacitor

Zhanjun Yu[□], Kanglei Xu, Erbin Liu, Xinlong Yao, Meng Wei, Yan Li, Jiehu Cui[□]

*School of Materials Science and Engineering, Zhengzhou University of Aeronautics,
Zhengzhou 450046, China*

* Corresponding author:

Zhanjun Yu: yuzhanjun@zua.edu.cn, Jiehu Cui: cuijiehu@zua.edu.cn

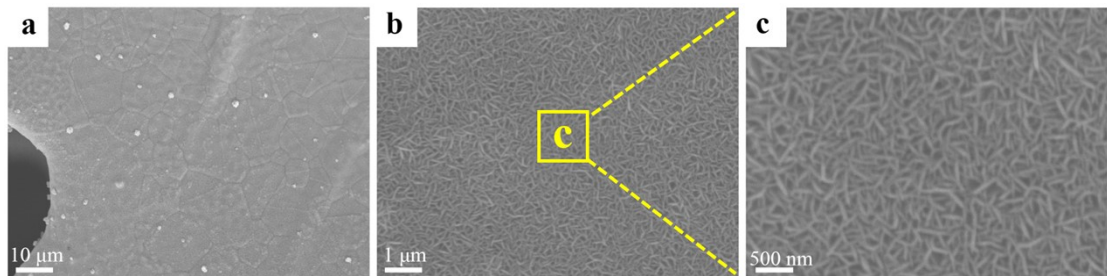


Fig. S1 SEM images of NiMn precursor at different magnifications.

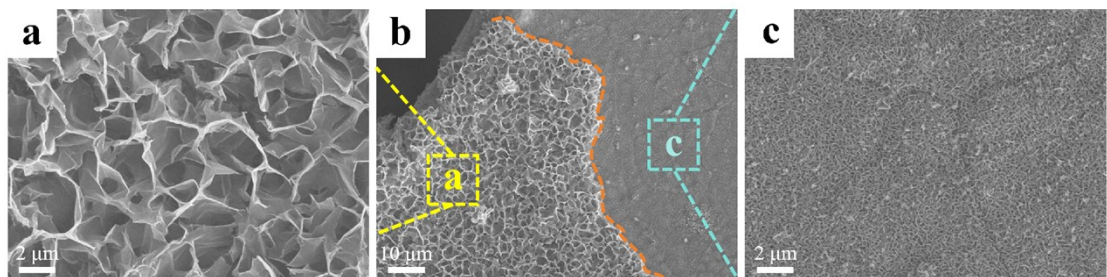


Fig. S2 SEM images of (a) a magnified view of the NMO phase on the surface of NMO@NCS, (b) the morphological features of NMO@NCS near its edge, and (c) a magnified view of the NCS phase on the surface of NMO@NCS.

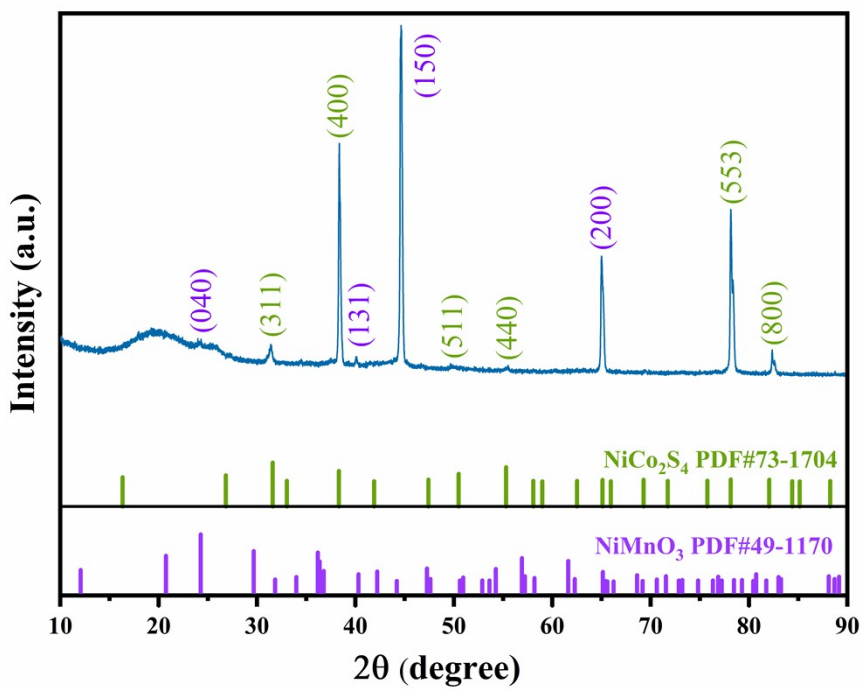


Fig. S3 XRD pattern of the NMO@NCS composite peeled off from the NF substrate

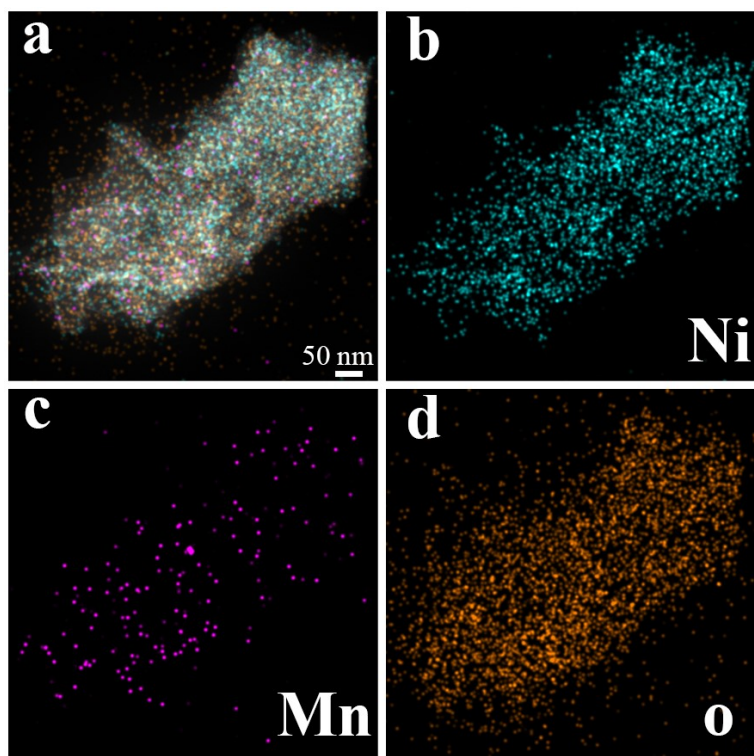


Fig. S4 EDS mapping patterns of NMO.

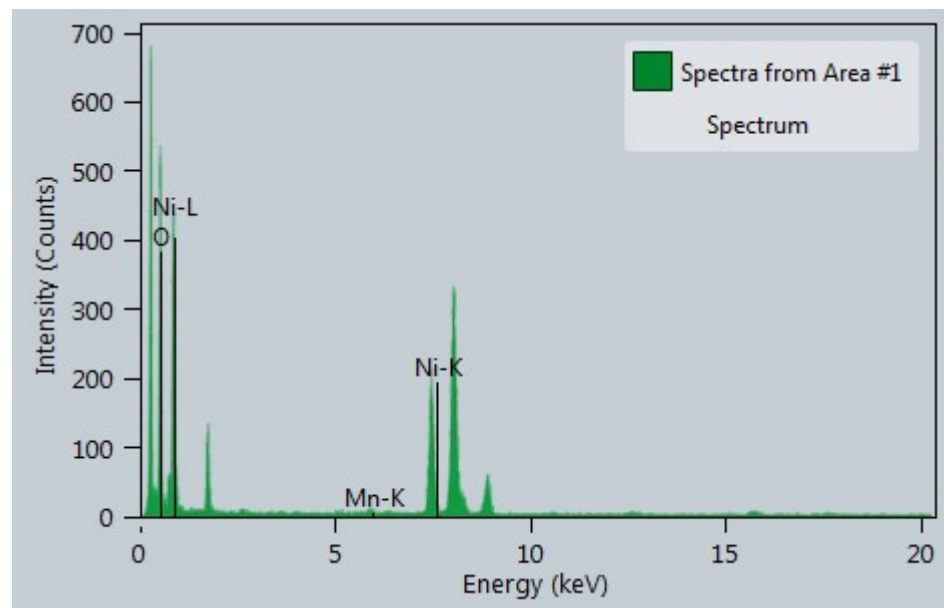


Fig. S5 EDS quantitative analysis spectra of NMO.

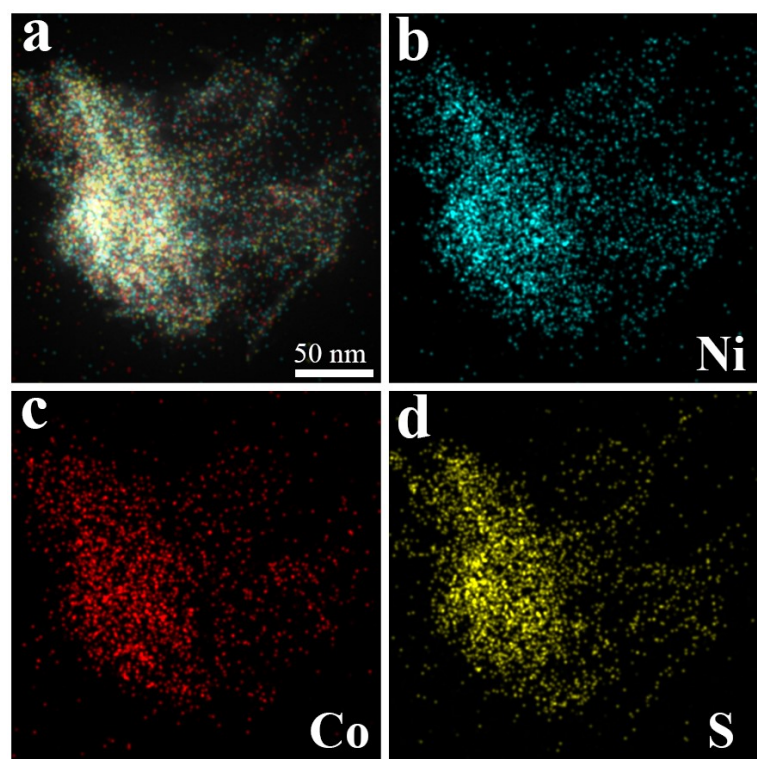


Fig. S6 EDS mapping patterns of NCS.

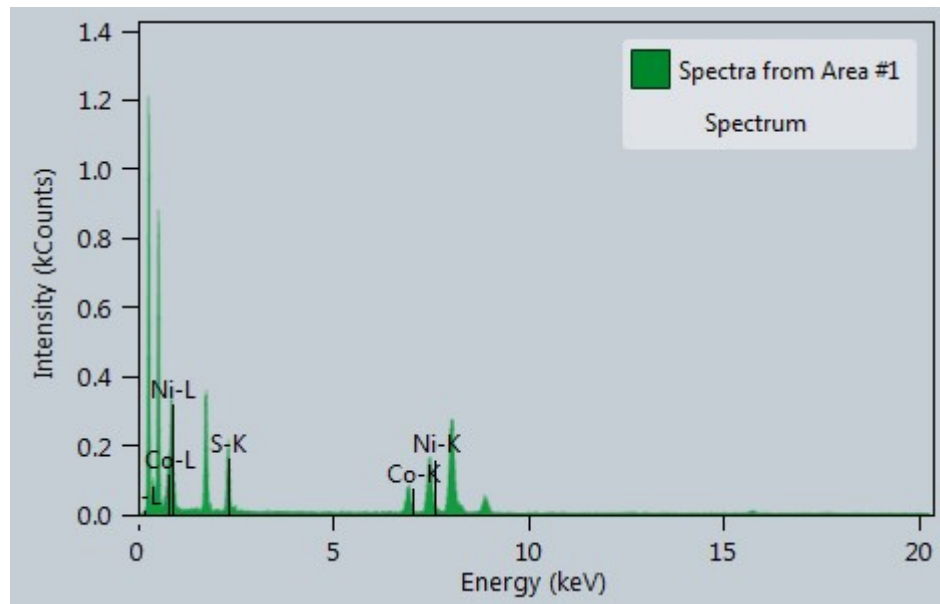


Fig. S7 EDS quantitative analysis spectra of NCS.

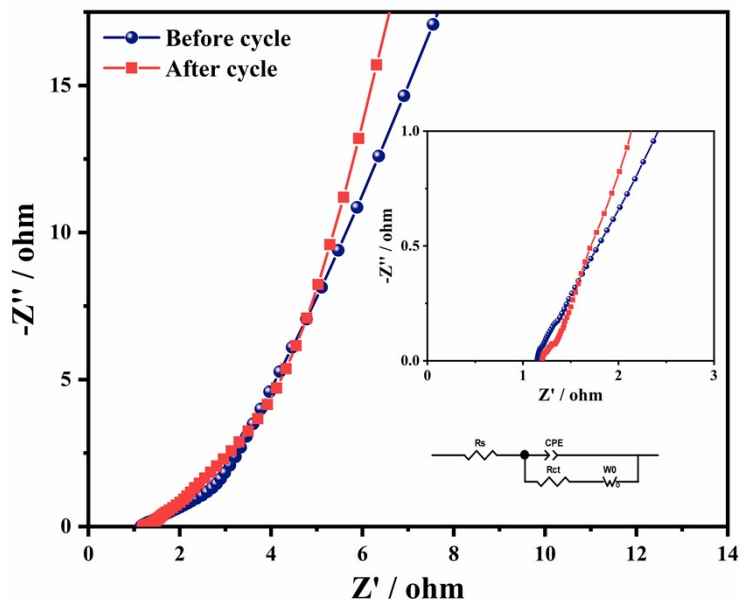


Fig. S8 Nyquist plots of NMO@NCS before and after 15,000 cycles at a current density of 20 A g^{-1} (the inset illustrates the enlarged view of the high-frequency and region equivalent circuit diagram).

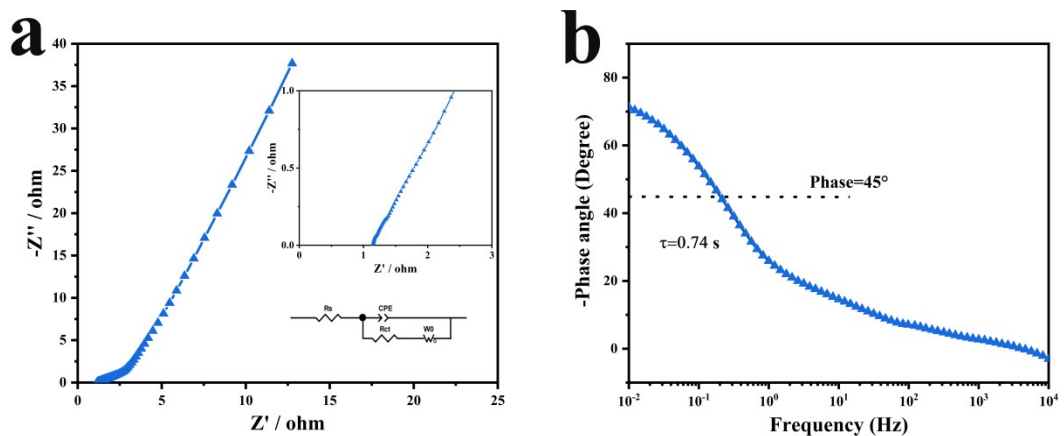


Fig. S9 (a) Nyquist plot and (b) Bode phase plot versus frequency of the NMO@NCS in three-electrode system.

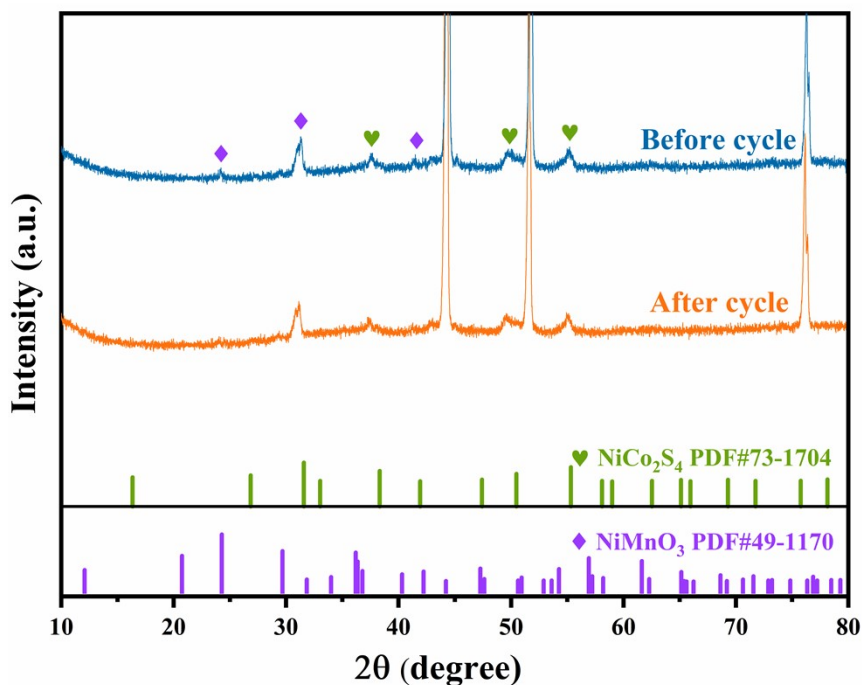


Fig. S10 XRD pattern of NMO@NCS electrode materials before and after 15,000 cycles.

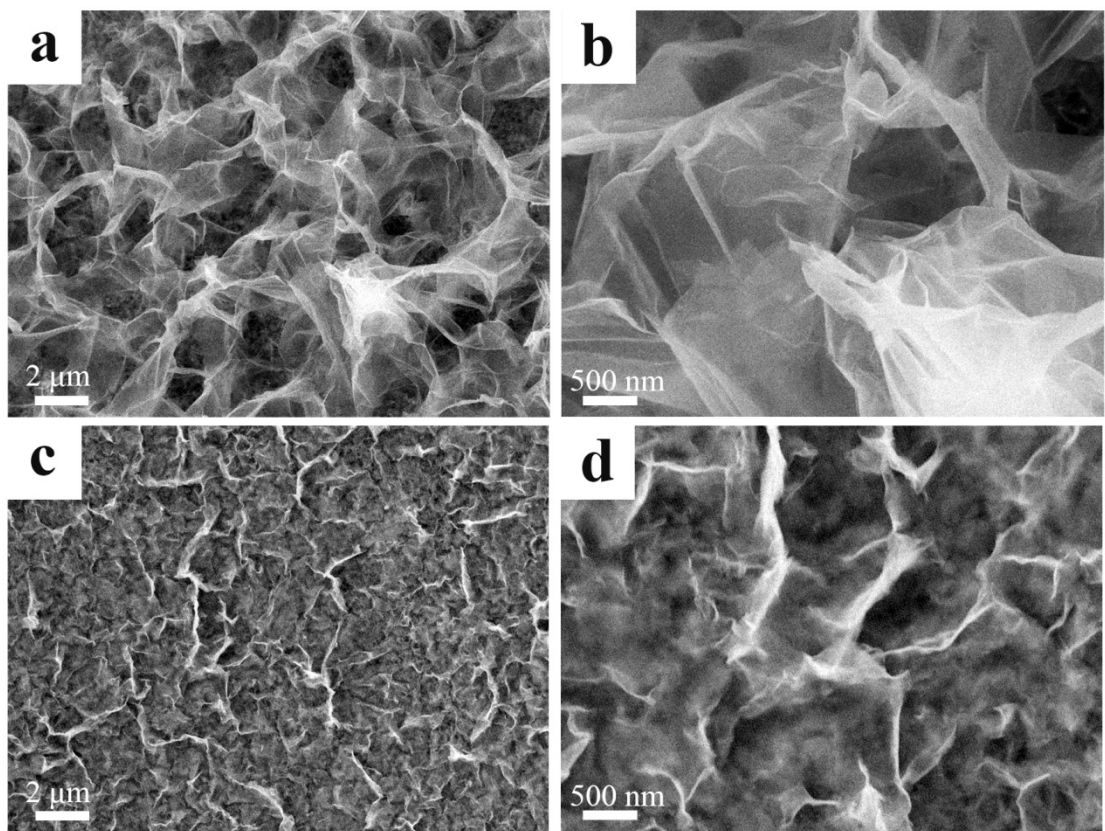


Fig. S11 FE-SEM images of NMO@NCS electrode materials before (a-b) and after (c-d) 15,000 cycles.

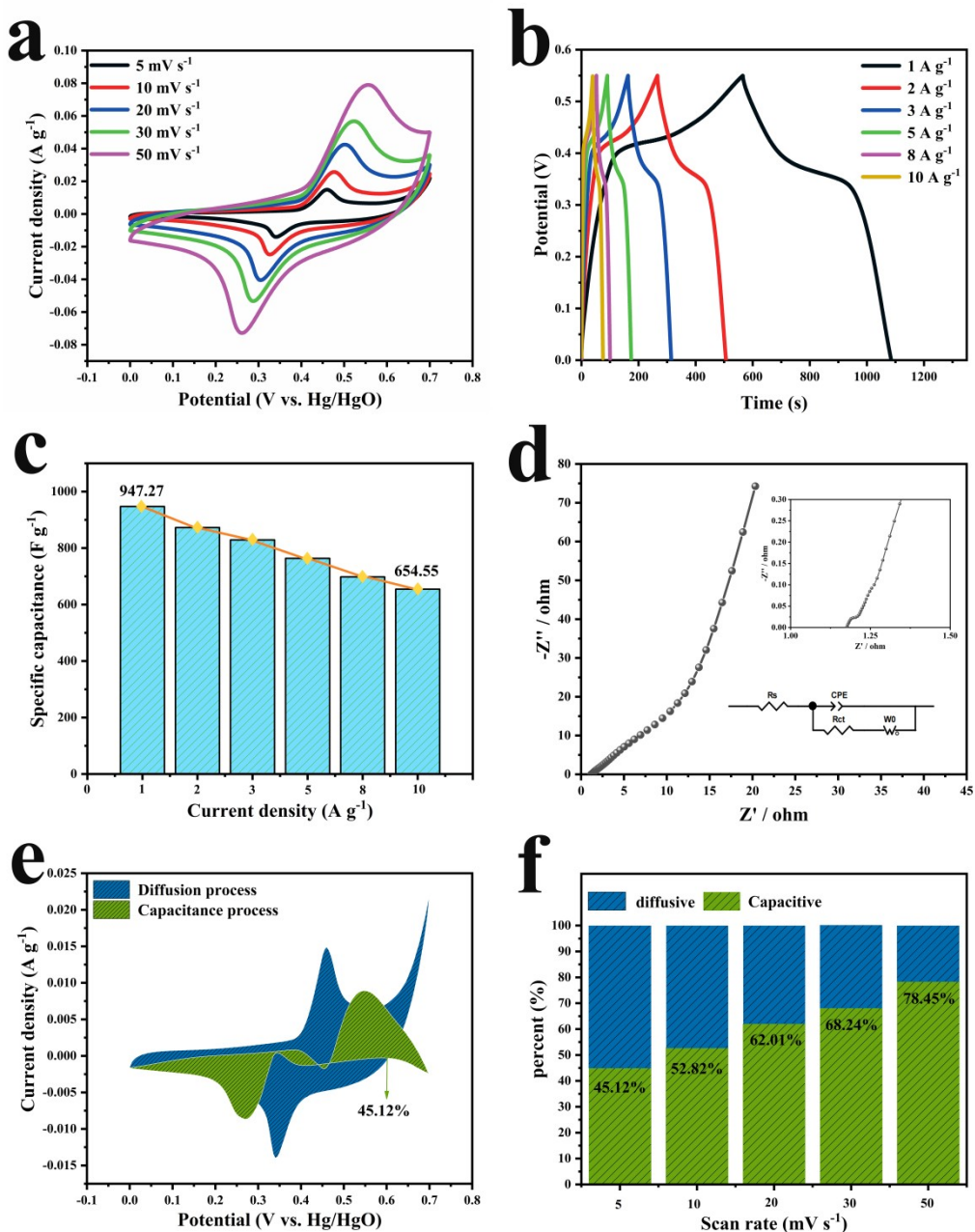


Fig. S12 (a) CV curves of NMO electrode at different scan rates. (b) GCD curves of NMO at various current densities. (c) The NMO histogram of Cs changes with current densities. (d) Nyquist plots of NMO (the inset shows the enlarged view of the high-frequency region and its equivalent circuit diagram). (e) Integral area diagram of the capacitive contribution and diffusion-controlled contribution processes to the charge storage for NMO electrode under a scan rate of 5 mV s^{-1} . (f) Histogram of the capacitance contribution and diffusion controll contribution of NMO at different scan rates.

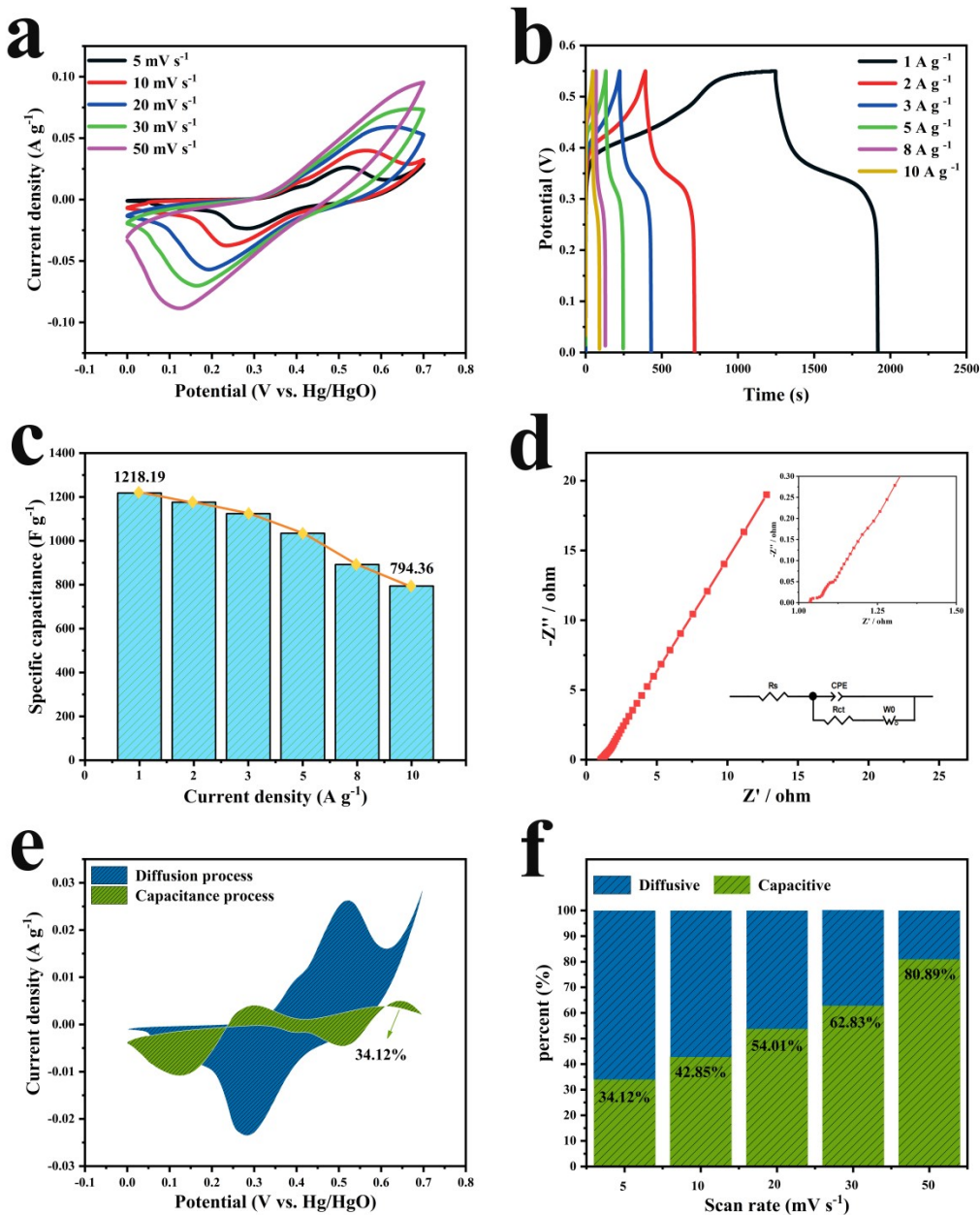


Fig. S13 (a) CV curves of NCS electrode at different scan rates. (b) GCD curves of NCS at various current densities. (c) The NCS histogram of Cs changes with current densities. (d) Nyquist plots of NCS (the inset shows the enlarged view of the high-frequency region and its equivalent circuit diagram). (e) Integral area diagram of the capacitive contribution and diffusion-controlled contribution processes to the charge storage for NCS electrode under a scan rate of 5 mV s^{-1} . (f) Histogram of the capacitance contribution and diffusion controll contribution of NCS at different scan rates.

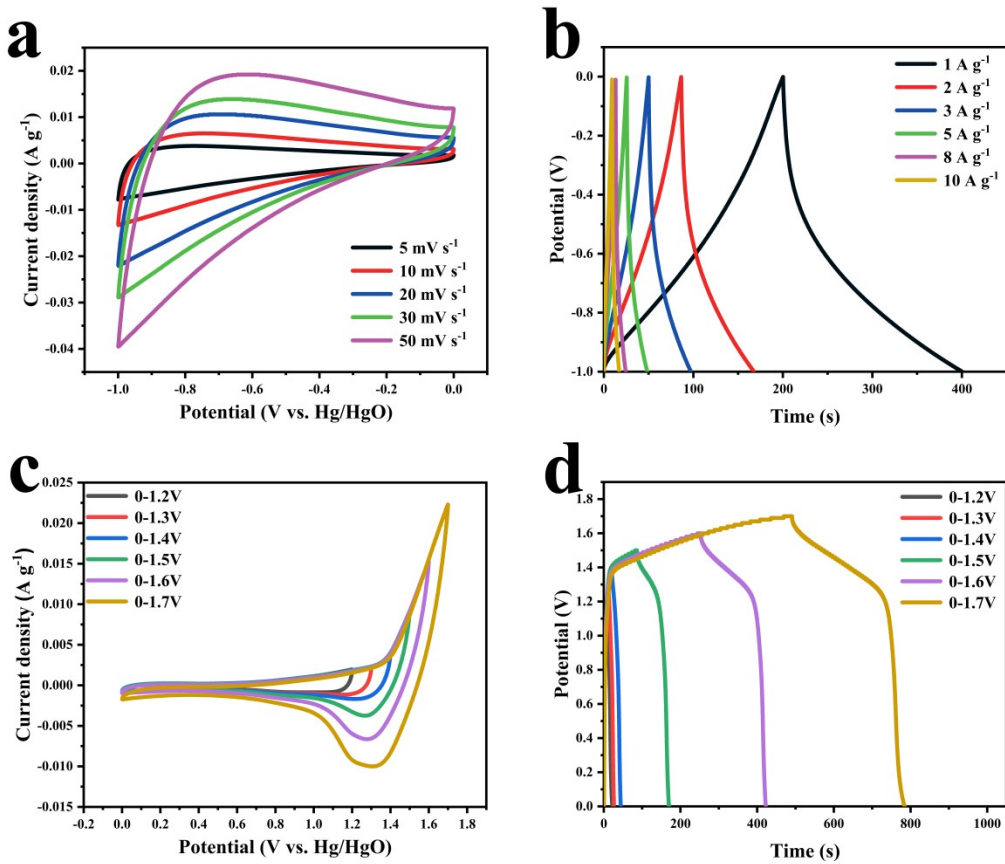


Fig. S14 (a) CV and (b) GCD curves of AC electrode material at different scan rates and current densities under the same voltage window. (c) CV and (d) GCD curves of assembled NMO@NCS//AC ASC device at the various potential windows varying from 0-1.2 V to 0-1.7 V.

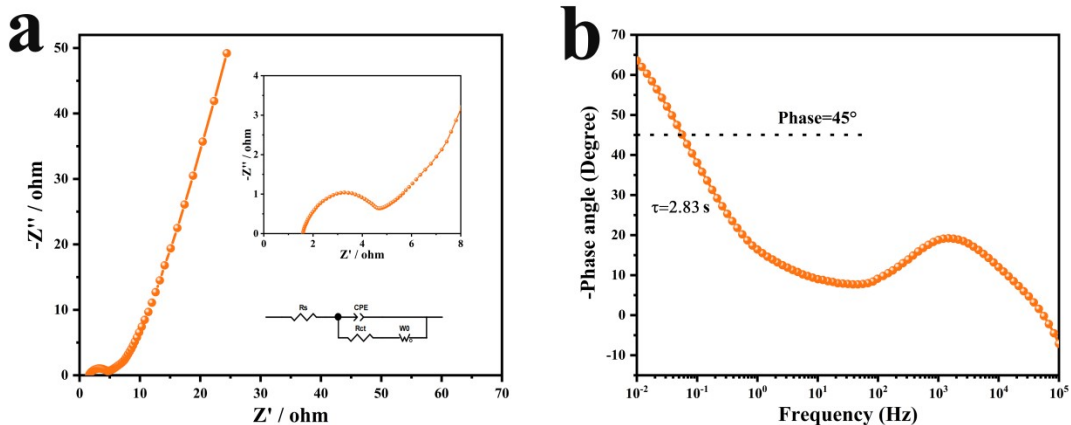


Fig. S15 (a) Nyquist plot and (b) Bode phase plot versus frequency of the NMO@NCS//AC ASC.

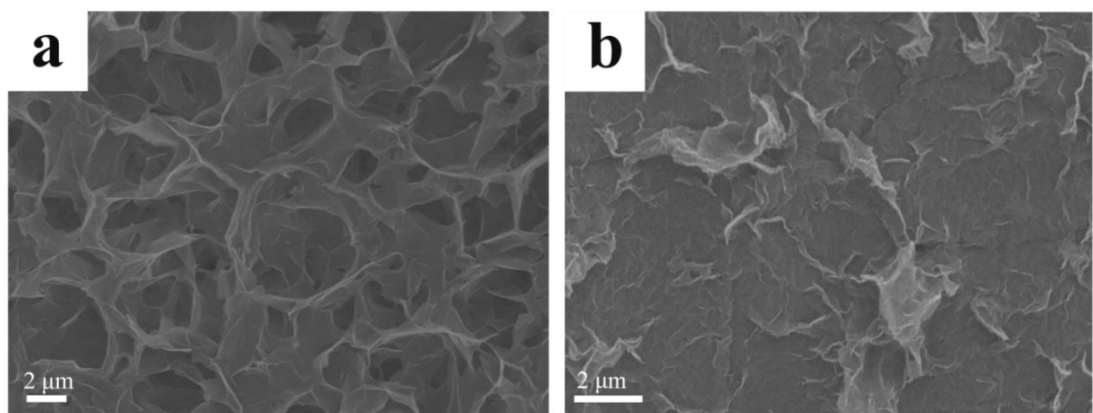


Fig. S16 SEM images of NMO@NCS electrode materials before (a) and after (b) 20,000 cycles.

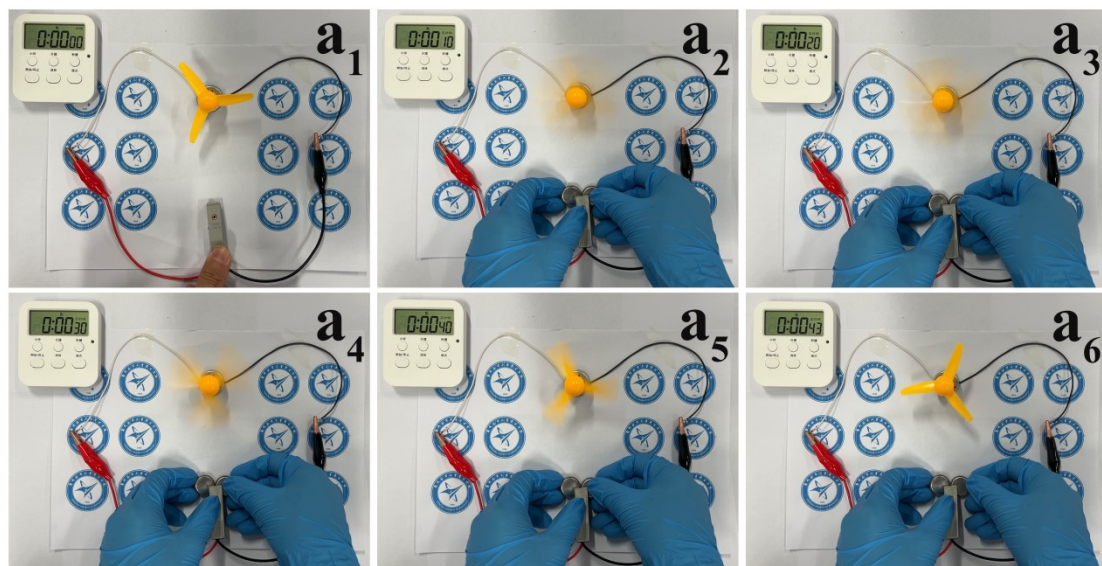


Fig. S17 Two NMO@NCS//AC ASC devices connected in parallel powering a min-fan.



Fig. S18 Two NMO@NCS//AC ASC devices connected in series light up the "ZUA" blue LED display.

Table S1 Triplicate ICP analyses of Mn and Co elements in the NMO@NCS.

Element	Total mass (g)	Element content ($\mu\text{g kg}^{-1}$)	Element content W(%)
Mn	0.0681	2238555.5653	0.2239%
Mn	0.0681	2249071.6593	0.2249%
Mn	0.0681	2292580.1909	0.2293%
Co	0.0681	5966264.2438	0.5966%
Co	0.0681	6019751.5051	0.6020%
Co	0.0681	6013407.1219	0.6013%

Table S2 Summary of Cs values (F g^{-1}) of all electrode materials vs. various current densities (A g^{-1}) based on GCD curves of all as-prepared samples. Values in parentheses are expressed in units of C g^{-1} .

	NMO	NCS	NCO@NCS
1	947.27 (521)	1218.19 (670)	2296.55 (1263.1)
2	872.73 (480)	1176 (646.8)	2225.82 (1224.2)
3	829.09 (456)	1124.18 (618.3)	2176.91 (1197.3)
5	763.64 (420)	1034.55 (569)	2072.73 (1140)
8	698.18 (384)	892.22 (490.72)	1917.09 (1054.4)
10	654.55 (360)	794.36 (436.9)	1825.45 (1004)

Table S3 Coulombic efficiency of NMO@NCS electrodes at varied current densities in a three-electrode system

Current density (A g^{-1})	Coulombic efficiency (%)
1	83.13
2	90.31
3	92.88
5	93.83
8	94.35
10	95.53

Table S4 Comparison diagram of C_s between this work and previously reported work for different materials.

Materials	Current density (A g ⁻¹)	C_s (F g ⁻¹)	Reference
NiMnO ₃ @NiCo ₂ S ₄	1	2296.55	This work
NiMnO ₃ /Ni ₆ MnO ₈	1	494.4	[56]
NiMn ₂ O ₄ @g-C ₃ N ₄	3	1530	[57]
ZnO/CoO@NiCoS	1	1868	[58]
NiCo-LDH@NiCoS@NiMnS	1.6	1862	[59]
NiMn ₂ O ₄ /CoS	1	1354.2	[60]
NiCo ₂ S ₄ @RGO	0.5	1804.7	[68]
g-C ₃ N ₄ @NiCo ₂ S ₄	1	1256	[69]
MWCNT-COOH@NiCo ₂ S ₄	2	1964.9	[70]

Table S5 A comparison of energy density and power density of the asymmetric supercapacitors reported in recent literatures.

Positive//negative electrode	Energy density (Wh·Kg ⁻¹)	Power density (W·kg ⁻¹)	Reference
NiCo ₂ S ₄ @CoAl-LDH	35.1	751.2	[65]
Ni-Mn-S@NiCo ₂ S ₄	59.1	344.8	[66]
NiMnO ₃ @NiO	28.1	750	[33]
NiCo ₂ S ₄ @RGO	24.4	750	[68]
g-C ₃ N ₄ @NiCo ₂ S ₄	16.7	1256	[69]
MWCNT-COOH@NiCo ₂ S ₄	33.6	375	[70]
NiMnO ₃	11.13	198.52	[38]
NiCo ₂ S ₄	38.2	400	[67]
NiMnO ₃ @NiCo ₂ S ₄	69.24	850.10	This work

References:

- 56 S. Qiao, N. Huang, Y. Zhang, J. Zhang, Z. Gao, S. Zhou, *Int. J. Hydrogen Energy*, 2019, **44**, 18351-18359.
 57 S. Vignesh, S. Suganthi, T. H. Oh, *Inorg. Chem. Commun.*, 2024, **167**, 112734.
 58 Y. He, X. Zhou, S. Ding, Q. Hu, D. Lin, X. Wei, *J. Alloy. Compd.*, 2021, **875**, 160046.
 59 D. Luo, J. Zou, B. Ma, Z. Wei, X. Ye, Y. Wu, L. Zhang, Q. Wang, L. Ma, *J. Alloy. Compd.*, 2024, **1004**, 175798.
 60 W. Chen, L. Yan, Z. Song, L. Xiao, *Electrochim. Acta*, 2024, **491**, 144329.
 65 J. Hu, Y. Pan, Q. Zhang, Z. Dong, S. Han, *Energy Fuels*, 2024, **38**, 6459–6470.
 66 L. Wan, Y. Yuan, J. Liu, J. Chen, Y. Zhang, C. Du , M. Xie, *Electrochim. Acta*, 2021, **368**, 137579.
 33 Y. Chen, L. Cao, P. Lian, J. Guan, Y. Liu, *J. Alloy. Compd.*, 2020, **832**, 154936.
 38 S. D. Dhas, P. S. Maldar, M. D. Patil, K. M. Hubali, U. V. Shembade, S. B. Abitkar, M. R. Waikar, R. G. Sonkawade, G. L. Agawane, A. V. Moholkar, *J. Energy Storage*, 2021, **35**, 102277.
 67 J. Tang, W. Huang, X. Lv, Q. Shi, *Nanotechnology*, 2020, **32**, 085604.
 68 Z. Li, X. Ji a, J. Han, Y. Hua, R. Guo, *J. Colloid Interface Sci.*, 2016, **477**, 46–53.
 69 Z. Li, L. Wu, L. Wang, A. Gu, Q. Zhou, *Electrochim. Acta*, 2017, **231**, 617–625.
 70 Z. Li, Y. Xin, H. Jia, Z. Wang, J. Sun, Q. Zhou, *J. Mater. Sci.*, 2017, **52**, 9661–9672.